RESEARCH ARTICLE

Control of a MEMS Fast Steering Mirror With Improved Quasi-Static Performance

YU ZIHAO[1,2], **WANG LIHAO**[1], **WANG YANG**[1], **ZHANG YONGGUI**[1], **LIU YICHEN**[1], **AND WU ZHENYU**[1,2,3,4]

[1]State Key Laboratory of Transducer Technology, Shanghai Institute of Microsystem and Information Technology, Chinese Academy of Sciences (CAS), Shanghai 200050, China
[2]University of Chinese Academy of Sciences, Beijing 100049, China
[3]Shanghai Industrial μTechnology Research Institute, Shanghai 201800, China
[4]School of Microelectronics, Shanghai University, Shanghai 200444, China

Corresponding authors: Wang Lihao (lhwang@mail.sim.ac.cn) and Wu Zhenyu (zhenyu.wu@mail.sim.ac.cn)

ABSTRACT This paper presents a control algorithm for a micro-electro-mechanical system (MEMS) fast steering mirror (FSM), whose performance is poor in open loop control mode. Based on the characterization and parameter identification of MEMS FSM, an improved double step algorithm is proposed to shorten the settling time and improve its quasi-static working bandwidth. A characterization system is set up, in which an optical sensor is utilized to monitor the tilt angle of FSM. The performance of the FSM in the time and frequency domain are both acquired, while the critical parameters of the FSM model are identified. Finally, the closed-loop experiments for the FSM are done to verify the effectiveness of the control algorithm. The experimental results demonstrate that the settling time (98%) of the FSM is effectively reduced from 398 ms to 0.4 ms under the improved double step control mode, which has a better tracking performance and tiny overshoot, compared with the open loop control mode.

INDEX TERMS MEMS, micromirror, tracking control, improved double step algorithm.

I. INTRODUCTION

Fast steering mirror (FSM) is an optical device for quickly and accurately adjusting the direction of the reflected laser, which, as a significant component, can therefore acquire and track the optical signal to provide a stable communication link [1], [2], [3], [4], [5]. FSM is mainly divided into voice coil motor FSM, piezoelectric ceramic FSM, and MEMS FSM. The eigenfrequency of the voice coil motor FSM is usually in the range of 100 Hz to 700 Hz [6]. Therefore, the voice coil motor is prone to resonate. The hysteresis is a difficulty for piezoelectric ceramic FSM control, which will become pronounced, especially under high driving voltages [7]. This characteristic leads to the nonlinearity of FSM, so a compensation algorithm is necessary to be implemented in the driver [8]. Micro-electro-mechanical system (MEMS)

The associate editor coordinating the review of this manuscript and approving it for publication was Mohammad Hossein Moaiyeri.

mirrors, as a class of integrated chip-based mirrors, can be flexibly designed in materials and structure for different applications. Thus, the MEMS FSM can be designed to avoid some of these difficulties in a certain scenario, and it is also utilized in inter-satellite laser communication [1], [2], [4]. To counteract the satellite jitter occurring in orbital flight [1], [3], whose frequency often ranges from 300 Hz to 500 Hz, FSM needs to respond with the control signal. Therefore, quasi-static working bandwidth is a key parameter of the FSM system, and it should be greater than 500 Hz, which reflects the speed of adjusting the laser pointing. High quasi-static working bandwidth requires a short settling time when the tilt angle changes from one degree to another.

To increase the working bandwidth and shorten the settling time of the FSM system, a proper driver and controller need to be developed and implemented. One category of methods is feedback control. Feedback methods need a high-speed sensor. For voice coil motor FSMs and piezoelectric ceramic

FSMs, the general angle sensors include optical sensors [9] and electrical sensors [10], [11]. Among them, the electrical sensor is usually installed inside the FSM, and it is relatively fast sensing. However, the relationship between the feedback signal and the angular signal is usually complex. The optical sensor is usually linearly related to the angular signal with a designed optical path, while it has a slower sensing rate. Due to the diversity of MEMS FSM structures, they can integrate some sensors, such as piezo-resistance sensors. References [12] and [13] and capacitive sensors [14], [15]. Their feedback signal is usually linear or quadratic in relation to the angular signal, and they are normally relatively fast sensing, as well. Nonetheless, there is a dilemma that it is difficult to lead the sensing signal out. What's more, an accurate modeling of the system is significant, as well. For example, Boston University reported a MEMS FSM [16]. It uses an overdrive algorithm to reduce its settling time and improve quasistatic performance. In addition, as a new type of MEMS device, the research on MEMS FSM is still under development.

The contribution of this paper is that an improved double step control algorithm is proposed to improve the quasi-static operating performance of the MEMS FSM. Additionally, a performance characterization system was built and part of the performance of a new MEMS FSM was measured. To miniaturize the FSM system, we use a designed Field Programmable Gate Array (FPGA) to implement algorithms instead of large controller box. A Position-sensitive-detector (PSD) sensor is adopted to collect the optical signal as angular signal for feedback. After constructing the FSM system, the close-loop experiments are conducted, and the experimental results are analyzed.

The paper is organized as follows. The structure features, operating principle, and modeling of the FSM are discussed in section II. Then, the improved double step algorithm is introduced in section III. Experimental results, parameters identification, and analysis of the test results are investigated in section IV. Finally, section V concludes this study.

II. FSM SYSTEM ANALYSIS
A. MEMS FSM STRUCTURE
This section presents a MEMS FSM. The FSM consists of a mirror and four actuators. They are fabricated on silicon substrate by the MEMS process. The piezoelectric actuators are fabricated by scandium-doped aluminum nitride (AlScN) film, which has the advantages of good linearity under small displacement, high working frequency, low delay, and no hysteresis and no creep [17], [18]. Thus, AlScN film is a proper actuator material for the quasistatic working mode of MEMS FSM. To facilitate experiments, the substrate of the chip is glued to a pre-designed PCB board using epoxy resin hot melt adhesive.

Fig.1(a) shows the transmission structure of the FSM, which is composed of four symmetrical cantilevers covered by AlScN film and silicon-based springs, which enhance the

(a)

(b)
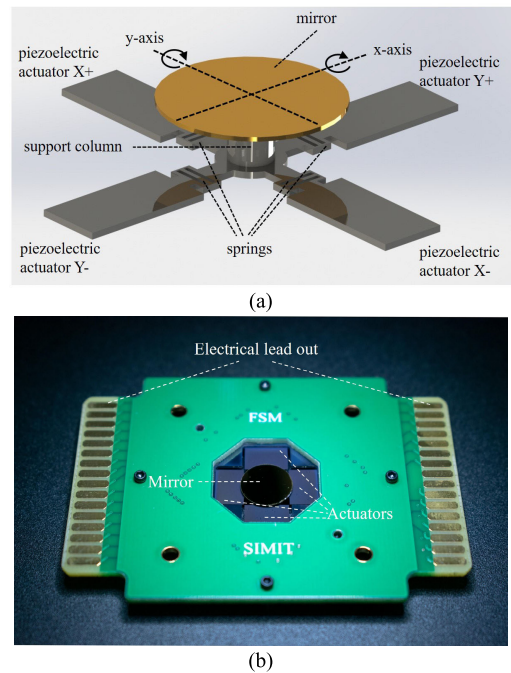
FIGURE 1. Overview of a MEMS FSM (a) the dynamic structure of the FSM in two axes (b) a picture of the FSM's test board.

TABLE 1. FSM parameters.

parameters	value
mirror diameter	10 mm
tilt angle	±4 mrad
chip size	25 mm × 25 mm × 1 mm
chip mass	0.5 g
input capacitance	< 10 nF
drive voltage	± 90 V
power consumption	< 10 μW

mm = millimeter, mrad = milliradian, g = gram, nF =nanofarad, V = volt, μW = microwatt

flexibility of the beams. The connection of the actuators and the mirror is a rigid joint with a support pillar. The springs can reduce the hardness of the beams and prevent the beams from damage by avoiding stress concentration and uniformly dispersing the stress over the beams. The piezoelectric actuators are connected to a specific driver circuit. When the driver circuit is working, an electric field is applied in the direction of the AlScN film's polarization, causing the beam to stretch and bend. As a pair of beams are bent in opposite directions at the same time, the support column will rotate. Therefore, the mirror tilts an angle following the support pillar. This is the operating mode in one axis. In addition, when two axes work together, the support column receives torsional moments in two orthogonal directions and transfers the torque to the mirror. Therefore, the mirror can be rotated in two orthogonal directions.

To characterize the FSM's performance, we designed a printed circuit board (PCB) to lead out the electronic pins of the FSM for the following experiments. The electronic

TABLE 2. Characteristic variables and equivalent variables.

FSM model		Equivalent model	
moment	M	force	F
moment of inertia	J	equivalent mass	m
tilt angle	θ	displacement	x
elastic coefficient	k	elastic coefficient	k
damping coefficient	b	damping coefficient	b
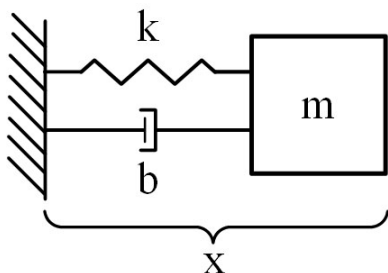
FIGURE 2. Equivalent dynamical model of FSM.

connection is realized by a gold wire bonding process. A picture of the final module is shown in fig. 1(b).

Here some key parameters are presented in tab.1. The significant advantages of the MEMS FSM are its small volume and mass. Thanks to the wafer-level technology, the thickness of MEMS FSMs is much smaller than traditional FSMs. Take PI's FSM as an example, the thickness of the voice coil motor FSM(V-931) and the piezoelectric ceramic FSM(S-330) are 26mm and 42mm [19], [20], but the MEMS FSM is only 1mm thick. Additionally, the masses of these FSMs are all greater than 500 g, which is more than one order of magnitude bigger than this MEMS FSM.

B. OPERATING PRINCIPLE

As explained above, the tilt angle of the mirror is affected by the bending of a pair of beams and springs in one rotation axis. To evaluate the tilt angle of the FSM, we first establish the kinetic equations of the FSM. Each axis of the FSM is essentially a spring-damped system. Taking the x-axis as an example, it can be equivalent to a simplified model in fig. 2. The relationship between the FSM kinetic model and the equivalent model is presented in tab.2. Here each row of two columns is equivalent.

According to the analysis in section II-A, when the beam is extended and bent, it provides moment M to the mirror through the spring, which is related to the tilt angular acceleration $\ddot{\theta}$, tilt angular velocity $\dot{\theta}$ and tilt angle θ. This process is similar to the compression and extension of the spring, so we use a spring with an elastic coefficient k, and a damper with a damping coefficient b to connect a mass m to express the dynamic process.

C. DYNAMIC ANALYSIS

With the analysis in section II-B, the dynamic equations of the harmonic oscillator model in fig.2 are expressed with (1) and (2).

$$m_1\ddot{x}_1 + b_1\dot{x}_1 + k_1x_1 = F_1, \tag{1}$$
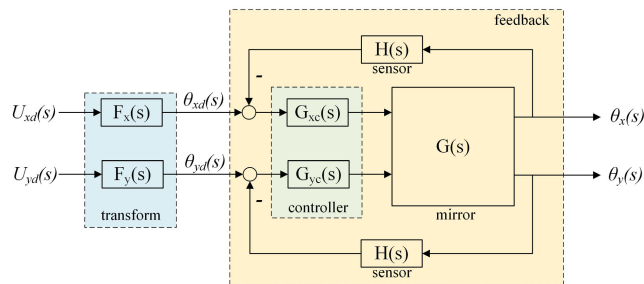
FIGURE 3. FSM system block diagram.

$$m_2\ddot{x}_2 + b_2\dot{x}_2 + k_2x_2 = F_2. \tag{2}$$

Thus, the equations of FSM can be obtained by analogy from the equivalent model. Further, the actual inputs of the FSM system are the voltage applied to the driver circuit for axes, so the relationship between the input torque and input voltage needs to be derived and measured. Considering the small angle of tilt θ, $cos\theta \approx 1$, the torque is $M \approx 2rF$, where r is the distance between the edge of the supporting column to the mirror center and F is the force applied to supporting column. By the structural characteristics and driven mode, the driving force and the driving voltage are approximately linear in a small tilt angle range [21]. The linear conversion coefficient is defined as c and the relationship can be written as: $M \approx rF = cV$. Consequently, the equations of FSM can be derived as follow:

$$J_x\ddot{\theta}_x + b_x\dot{\theta}_x + k_x\theta_x = c_xV_x, \tag{3}$$
$$J_y\ddot{\theta}_y + b_y\dot{\theta}_y + k_y\theta_y = c_yV_y. \tag{4}$$

Because the MEMS FSM is an integrated device and the bending of the cantilever and the tilt angle of the mirror are tiny, some paraments such as the moment of inertia of the mirror and the elastic coefficient of springs are difficult to obtain. To design experiments for system identification, we use another set of parameters in (5) and (6) which are derived from (3) and (4). Here ω_n is the mirror's natural angular frequency; ζ is the damping ratio; K is the conversion coefficient between voltage and tilt angle. These equations are derived as follows:

$$\omega_{nx} = \sqrt{k_x/J_x}, \zeta_x = \frac{b_x}{2\sqrt{k_xJ_x}}, K_x = c_x/J_x; \tag{5}$$

$$\omega_{ny} = \sqrt{k_y/J_y}, \zeta_y = \frac{b_y}{2\sqrt{k_yJ_y}}, K_y = c_y/J_y. \tag{6}$$

III. ALGORITHM DESIGN

From the analysis in section II, the FSM can approximate a second-order system with damping. This system will oscillate when the input voltage is a step voltage. To reduce the oscillation and smooth the step response, the settling time should be as short as possible, and the overshoot should be small. Hence, it is necessary to design an appropriate algorithm according to the model of FSM. Here an improved double step algorithm is presented.

(a)

(b)
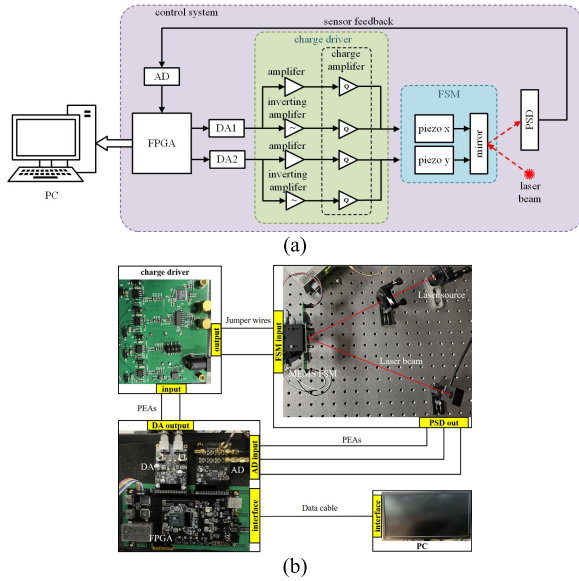
FIGURE 4. (a) FSM system schematic diagram. (b) picture of the FSM system. A specially designed charge driver is employed to drive two axes of FSM. PSD is used to detect the reflected light displacement.
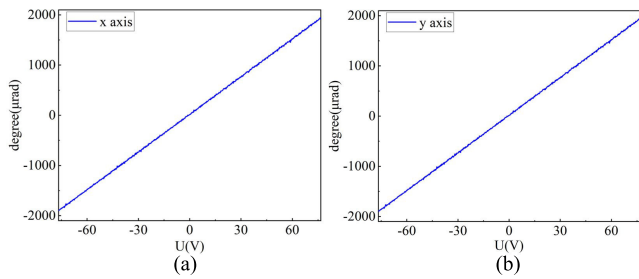
FIGURE 5. Two axes tilt angle. (a) Apply voltage V_x to the x-axis, the blue line is θ_x, K_x is the scale coefficient of V_x to θ_x. (b) Apply voltage V_y to the y-axis, the blue line is θ_y, K_y is the scale coefficient of V_y to θ_y.

First, considering input voltage, the output can be derived from the state space model. When a step voltage applied to the x-axis is $V_x(t < 0) = 0$, $V_x(t > 0) = V_0$, the output θ_x will approach harmonic oscillation in the first few periods. The solution to (3) is shown in (7):

$$\theta_x(t) = K_x V_x (1 - \exp(-\zeta_x \omega_{nx}) / \sqrt{1 - \zeta_x^2}$$
$$\times (sin(\omega_{nx}\sqrt{1 - \zeta_x^2} t + \varphi)), \qquad (7)$$

where $\varphi = arctan\left(\zeta_x \sqrt{1 - \zeta_x^2}\right)$. V_0 is the voltage required to reach and stay at the steady angle θ_{x0} after all oscillations have subsided [22], [23].

The period of the oscillation ringing in step response(T_0) is derived from (7) as follow:

$$T_0 = 2\pi / \omega_{nx}\sqrt{1 - \zeta_x^2}, \qquad (8)$$

and the maximum overshoot will appear in $T_0/2$ without zero angle velocity, as the overshoot $\sigma\%$ should approach 100% as $\zeta_x \to 0$ from (8).
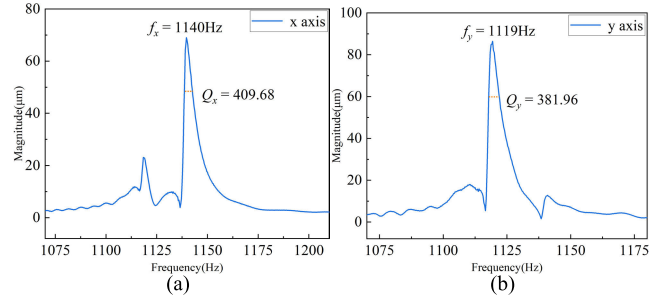
FIGURE 6. Piezoelectric beams deflection with different frequencies voltage input. The input voltage is 300 V chirp signal sweep from 300 Hz to 2000 Hz. (a) The blue lines are the frequency response of the x-axis. (b) The blue lines are the frequency response of the y-axis. Q_x and Q_y are quality factors of the x-axis and the y-axis.

To decrease the overshoot and access to a steady state rapidly, a double step derive method is adopted in the controller. In the first step, the input voltage is $V_0' + (V_0 - V_0')/2$, where V_0' is the previously demanded voltage, and V_0 is the current demanded voltage. When the tilt angle at the maximum overshoot with the first step, change the input voltage to the double amplitude to the demanded voltage (V_0) and hold on, which is the second step. At the time voltage changes, the overshoot of the first step approaches the steady state tilt angle (θ_{x0}) for the demanded voltage (V_0). The double voltage holds the tilt angle on, so the oscillation is avoided. This method takes advantage of overshoot and avoids ringing. Therefore, the original step input voltage becomes:

$$V_x = \begin{cases} V_0' & (t \leq 0), \\ V_0' + (V_0 - V_0')/2 & (0 < t \leq T_0/2), \\ V_0 & (t > T_0/2). \end{cases} \qquad (9)$$

The system parameters may change slightly during the operation of the FSM, because of the environmental disturbance. Therefore, the demanded voltage, matching the demanded tilt angle, may be changed. In this case, if the last input voltage is also (V_0), the output tilt angle will become θ_{x0}'. There will produce an error ($e = \theta_{x0} - \theta_{x0}'$). To correct the error, a feedback loop is necessary. Here a PSD sensor is selected as a feedback sensor.

According to the analysis above, the output tilt angle and input voltage can be derived from each other in equation (10) when the FSM is in a steady state:

$$\theta_{x0} = k_x V_{x0}. \qquad (10)$$

Thus, once the PSD sensor collected the feedback signal and sends it back to the processor, the desired angle is updated to $\theta_x = \theta_{x0} + e$ and sent it to the controller. Then, the double step controller will output the new voltage to the mirror, and the error will be reduced.

The FSM control system's block diagram is given in fig.3. Here $\theta_d(s)$ is the desired tilt angle; $U_d(s)$ is the setting scanning track. The double step controller is placed in the $G_c(s)$ position. Moreover, $G(s)$ represents the FSM and $H(s)$ represents the angle sensor.
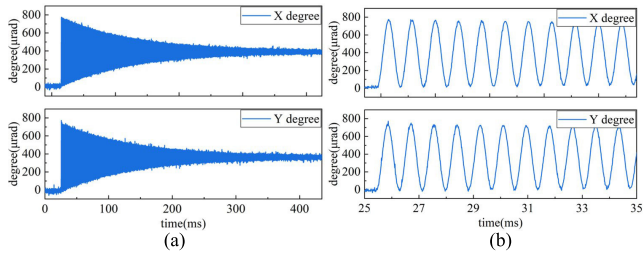
FIGURE 7. Step response of two axes. (a) The input is 33 V step voltage separately applied to two axes. The blue lines are the θ_x response and θ_y response to this input. (b) A closer look at the response when the tilt angle has changed.

TABLE 3. System parameters.

parameter	value
ω_{nx}	7162.8 rad/s
ω_{ny}	7030.9 rad/s
ζ_x	1.22×10^{-3}
ζ_y	1.22×10^{-3}
K_x	1.308×10^5 rad$^3 \cdot$s$^{-2} \cdot$V^{-1}
K_y	1.217×10^5 rad$^3 \cdot$s$^{-2} \cdot$V^{-1}

V = volt, s = second, rad = radian
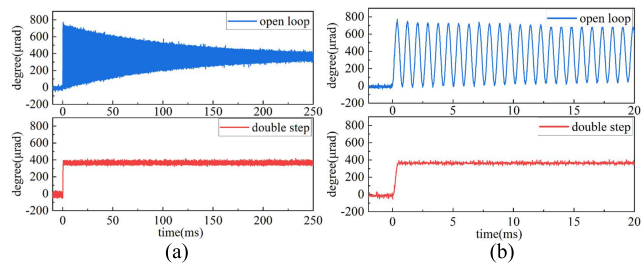
FIGURE 8. Step response of the x-axis in different control modes. (a) The input signal is 33V step voltage, θ_x response in open loop and double step control. (b) a closer look at the response for these control modes.

TABLE 4. Step response parameter.

control method	settling time (98%)	Maximum overshoot
open loop	398 ms	71.4%
improved double step	0.4 ms	0.3%

ms = millisecond

IV. EXPERIMENT AND RESULTS

A. EXPERIMENTAL SETUP

To investigate the FSM system performance, identify parameters, and verify the effectiveness of the designed algorithm, an angle test system is given in fig. 4. This system consists of FPGA, a driver circuit, FSM, and an angle test module. Because large amount of high-precision data need to be transmitted in a short period of time, FPGA that can communicate
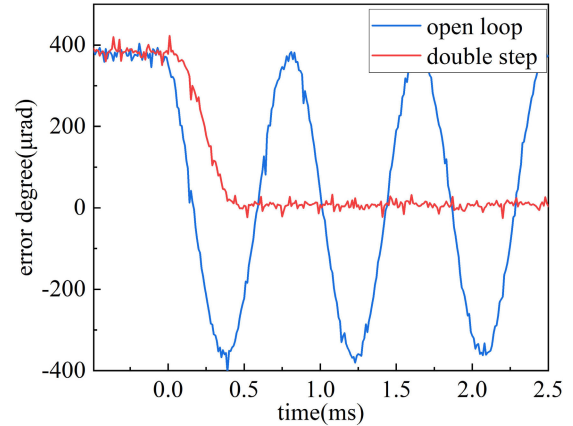
FIGURE 9. Error in step response from the desired degree and actual degree for different control modes. The error degree decays to from 400 μrad to 5 μrad at 0.4 ms under the improved double step control, while the mirror still oscillates under the open loop control.
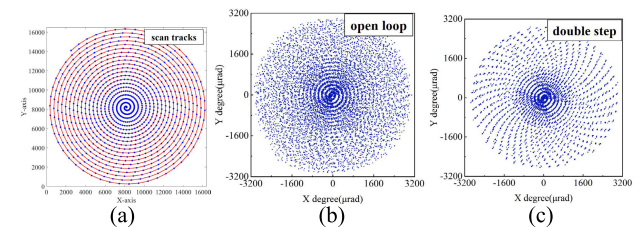
FIGURE 10. Spiral scan of two axes in different control modes. (a) The desired scan path is the red line. The blue spots are the desired tilt angles in two axes. The horizontal and vertical coordinates are their 14-bit DA values, which is stored in the ROM of the FPGA. (b) The blue spots are the actual scan tilt angles in two axes under open loop control. (c) The blue spots are the actual scan tilt angles in two axes under improved double step control.
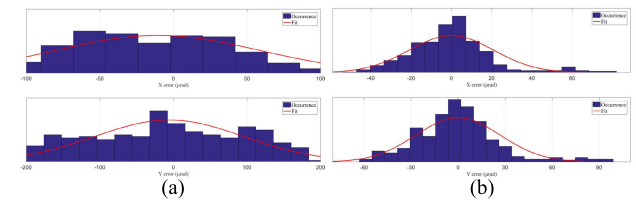
FIGURE 11. Error distributions of the spiral scan of two axes in different control modes. The upper part of each diagram is the x-axis distribution, and the down bottom part is the y-axis distribution, (a) error distributions under open loop control (b) error distributions under improved double step control.

in parallel is a suitable digital processing module. Besides, the algorithm proposed is easy to code in Verilog. All calculations and data transformations are implemented in FPGA (ARTIX-7 series, Xilinx), including feedforward compensation, signal conversion, and feedback control algorithm. After calculations, the control voltage is converted to drive voltage through the DA module from the controller in FPGA. Each axis is equipped with two opposite charge drivers. The angle test module is composed of a laser source, FSM bracket, and position-sensitive detectors (PSD, PDP90A, Thorlabs). Moreover, the light spot movements are measured from the PSD. Thus, FSM's tilt angle can be calculated by geometrical optics. FPGA receives PSD's feedback signal through the AD module and converts displacement to angle for control

TABLE 5. Comparison of key parameters in different FSMs.

institution	actuating structure	working bandwidth	maximum deflection angle	minimum angle resolution	repositioning accuracy
this work	MEMS	1500 Hz	2 mrad	5 μrad	26.8 μrad
Fraunhofer Institute for Photonic Microsystems, Germany[12]	MEMS	350 Hz	150 mrad	1.7 mrad	87 μrad
Automation and Control Institute, Austria[14]	MEMS	1000 Hz	253 mrad	-	300 μrad
Hamamatsu, Japan[24,25]	MEMS	150 Hz	262 mrad	-	170 μrad
Physik Instrumente, Germany[20]	piezoelectric ceramic	1300 Hz	2 mrad	0.5 μrad	0.15 μrad
Cedrat Technologies sa, France[3]	voice coil motor	2000 Hz	2.1 mrad	2 μrad	1.8 μrad

Hz = hertz, mrad = milliradian, μrad = microradian

algorithm calculation. Meanwhile, the angular signal and scanning track are upload to the PC for display.

B. PERFORMANCE CHARACTERIZATION AND PARAMETERS IDENTIFICATION

To identify the parameters in the state space model, the time domain characteristics and frequency domain characteristics of the FSM need to be measured. The relationship between the output tilt angle and the input voltage is shown in fig.5. As can be seen from fig.5 (a), the applied voltage ranges from −0.7 V to 0.7 V while the x-axis tilt angle follows the voltage. This test result is observed in the other axis in fig.5(b) as well. Overall, the output tilt angle can be approximately linear to the input voltage. And the scale coefficients of the two axes are very close. In conclusion, the experimental results agree with the dynamic analysis that the relationship between the moment applied to the mirror and the driving voltage is approximately linear.

Fig.6 and fig.7 show the dynamic performance of FSM in the frequency domain and time domain. The frequency characteristic is tested by Laser Doppler Vibrometer (LDV). A periodic chirp voltage is applied to the FSM as input voltage and LDV detects the vertical displacement of the mirror's edge. From fig.6 the characteristic frequencies of the two axes are $f_x = 1140$ Hz and $f_y = 1119$ Hz. The cutoff frequencies are close to the peak frequency and the quality factor Q of the FSM system is high. The quality factor Q is the quotient of the characteristic divided by the difference between the two cutoff frequencies.

For a second-order oscillatory system, the damping ratio ζ is proportional to the inverse of the quality factor Q and the oscillation will be violent if the ζ is small. Therefore, the step response should have a large overshoot and slow decay speed, as shown in fig.7. The settling time (5%) of the two axes is both 398 ms and the maximum overshoot of the two axes is 71.4% for the x-axis and 70.2% for the y-axis. In addition, both oscillation periods are around 0.9 ms from fig.7 (b), so the oscillation frequencies are approximately 1110 Hz, matching the frequency response.

The parameters of the state space model can be identified from the result of the above experiments and the specific numerical values are given in tab.3. The $\zeta = 1/(2Q)$ is on the order of 10^{-3}, so $\omega_n = 2\pi f \sqrt{1 - \zeta^2} \approx 2\pi f$ is derived from Fig.6. Furthermore, K is fitted from the data of Fig.5 and Fig.7.

C. EXPERIMENTAL RESULTS

Based on the state space model eqs. (5), and (6) and the results of system identification tab.3, the T_0 is configured to 0.891 ms in double step controller. A variable is used in the program to record the last set value. The error is only calibrated if the set value is stable. Besides, the frequency of error correction is less than half of T_0. Since the AD and DA have the upper limit of the sampling frequency, we use difference instead of differentiation and accumulation instead of integration.

Comparing the control results shown in fig.8 and fig.9, and summarized in tab.4. The double step algorithm improves the quasi-static performance of the FSM system. From fig.8 we can find that the improved double step controller, which resembles a high-performance filter, can eliminate the oscillation. The parameters of this algorithm should be highly accurate relying on the precise model, otherwise the oscillation will still be presenting, and the settling time will be longer. Moreover, fig.9 illustrates that the improved double step controller can decays the steady-state tracking error of the step response to within 5% under 2ms. Thus, the quasi-static working bandwidth, which is the reciprocal of the settling time, improves to over 500 Hz.

Furthermore, fig.10 and fig.11 show that the two control methods are compared for two-dimensional scanning with desired scan tracks. The desired scan track path is a spiral scanning curve shown in fig.9(a), covering the entire scanning range as far as possible. The coordinates of each desired tilt angle are entered with 1 second dwell to simulate quasi-static working mode. At the same time, the actual scanned values were sampled at every 2 ms intervals to observe the quasi-static working performance of the FSM at 500 Hz. From fig.10(b) and (c), the two-dimensional scan points are distributed in the vicinity of the set coordinates. Nevertheless,

the open loop scan points are so dispersed that the desired tracks are barely visible. In addition, fig.11 represents that the error distributions, where the RMS error mean square error for the x-axis and it for the y-axis in the open loop control scan are 278.02 μrad and 319.02 μrad. In contrast, the RMS error for the x-axis and it for the y-axis in the improved double step control scan are 20.96 μrad and 26.85 μrad. In addition, the error distributions are more concentrated in the improved double step control mode rather than open loop control mode.

In addition, some key parameters selected of different FSMs are compared in tab.5. In the field of MEMS FSM, few designs are aimed at quasi-static work with high precision pointing. Therefore, this MEMS FSM have high resolution compared with other study of MEMS FSMs with some sacrifices in the deflection range. Moreover, conducive to assistance of the control system for this MEMS FSM, the working bandwidth of this work can reach the same level as the mature traditional FSMs.

V. CONCLUSION

MEMS FSMs are appropriate actuators in laser pointing and communication systems because they are miniature, easy to control, and require few resources of a satellite platform. MEMS FSMs for this application need a unique design and proper control system to increase their precision and quasi-static working bandwidth. Thereby, a small range of the deflection angle range structure is utilized for those FSMs.

Furthermore, we have introduced a MEMS FSM based on cantilever beams support structure. This kind of structure will oscillate when stimulated by a sudden change signal [17]. The improved double step control method is suitable to utilize when the resonant frequency can be measured. This method can eliminate the oscillation and shorten the settling time. Compared with other methods such as PID control or sliding mode control, this controller requires mere one parameter to be adjusted which is the second step time, which is the outstanding advantage.

In this paper, a MEMS FSM and a measurement and control system are presented. Firstly, the structure and operating principle of the FSM are analyzed. Then, a mathematical model of the system is established. Further, a performance measurement system for the FSM is built and the FSM's performance is characterized. From experimental results, the tilt angle of the FSM is quite linear with the drive voltage. Furthermore, the FSM has a characteristic frequency of over 1000 Hz with quality factors approximating 400, which means the FSM is not prone to resonate at working frequencies below 500 Hz. After that, we proposed an improved double step algorithm and conducted experiments to verify the control effect. The control algorithm experimental results validate that the improved double step controller can significantly shorten the settling time. The double step controller shortens the settling time (98%) from 398 ms to 0.4 ms. Additionally, two-dimensional scanning experimental results indicate that the improved double step control mode has higher tracking accuracy than the open loop control mode. The RMS error of each axis is almost reduced by more than one order of magnitude. In conclusion, the improved double step algorithm significantly improved the quasi-static performance of this MEMS FSM.

In the future, an on-chip integrated piezoresistive sensor will be applied to detective the feedback signal, which will improve the stability of the closed-loop control. Then the study of multiple MEMS FSM systems of laser targeting will be conducted. Some more robust control algorithms will be utilized in this system.

REFERENCES

[1] O. Čierny and K. L. Cahoy, "On-orbit beam pointing calibration for nanosatellite laser communications," *Proc. SPIE*, vol. 58, no. 4, Nov. 2018, Art. no. 041605.

[2] M. Taylor, A. Roychowdhury, S. Maldonado, O. Zeng, S. Tuck, M. Adamkiewicz, S. Roy, J. Hillard, M. Radhakrishnan, and S. D'Amico, "Polar orbiting infrared tracking receiver (POINTR)," in *Proc. IEEE Aerosp. Conf.*, Mar. 2019, pp. 1–13.

[3] S. Hugi, T. Maillard, A. Baillus, G. Aigouy, O. Sosnicki, and F. Barillot, "Fine steering mirror based on piezo actuators: A point ahead mechanism (PAM30) for deep space optical communication module of the Psyche mission," *Proc. SPIE*, vol. 11852, Jun. 2021, Art. no. 118525N.

[4] S. Jeon and H. Toshiyoshi, "MEMS tracking mirror system for a bidirectional free-space optical link," *Appl. Opt.*, vol. 56, no. 24, pp. 6720–6727, 2017.

[5] P. Grenfell, A. Aguilar, and K. Cahoy, "Pointing, acquisition, and tracking for small satellite laser communications," in *Proc. 32nd Annu. AIAA/USU Conf. Small Satell.*, 2018, pp. 1–7.

[6] T. Shinshi, D. Shimizu, K. Kodeki, and K. Fukushima, "A fast steering mirror driven by voice coil motors and supported by magnetic suspension," in *Proc. 23rd Int. Conf. Mechatronics Technol. (ICMT)*, Oct. 2019, pp. 1–4.

[7] M. Bazghaleh, S. Grainger, and M. Mohammadzaheri, "A review of charge methods for driving piezoelectric actuators," *J. Intell. Mater. Syst. Struct.*, vol. 29, no. 10, pp. 2096–2104, Jun. 2018.

[8] Y. Chen, J. Qiu, J. Guo, and Z. Ying, "A charge controlled driving power supply for hysteresis compensation of piezoelectric stack actuators," *Int. J. Appl. Electromagn. Mech.*, vol. 59, no. 1, pp. 281–290, Mar. 2019.

[9] E. Csencsics, J. Schlarp, T. Schopf, and G. Schitter, "Compact high performance hybrid reluctance actuated fast steering mirror system," *Mechatronics*, vol. 62, Oct. 2019, Art. no. 102251.

[10] J. Zhong, R. Nishida, and T. Shinshi, "Design and precision tracking control of a high-bandwidth fast steering mirror for laser beam machining," *Precis. Eng.-J. Int. Societies Precis. Eng. Nanotechnol.*, vol. 73, pp. 128–139, Jan. 2022.

[11] D. J. Kluk, M. T. Boulet, and D. L. Trumper, "A high-bandwidth, high-precision, two-axis steering mirror with moving iron actuator," *Mechatronics*, vol. 22, no. 3, pp. 257–270, Apr. 2012.

[12] R. Schroedter, M. Schwarzenberg, A. Dreyhaupt, R. Barth, T. Sandner, and K. Janschek, "Microcontroller based closed-loop control of a 2D quasi-static/resonant microscanner with on-chip piezoresistive sensor feedback," *Proc. SPIE*, vol. 10116, Feb. 2017, Art. no. 1011605.

[13] R. Schroedter, T. Sandner, K. Janschek, M. Roth, and C. Hruschka, "Real-time closed-loop control for micro mirrors with quasistatic comb drives," *Proc. SPIE*, vol. 9760, Mar. 2016, Art. no. 976009.

[14] D. Brunner, H. W. Yoo, and G. Schitter, "Precise phase control of resonant MOEMS mirrors by comb-drive current feedback," *Mechatronics*, vol. 71, Nov. 2020, Art. no. 102420.

[15] D. Brunner, H. W. Yoo, and G. Schitter, "Linear modeling and control of comb-actuated resonant MEMS mirror with nonlinear dynamics," *IEEE Trans. Ind. Electron.*, vol. 68, no. 4, pp. 3315–3323, Apr. 2021.

[16] C. Pollock, "Extreme angle, tip-tilt MEMS micromirror enabling full hemispheric, quasi-static optical coverage," *Opt. Exp.*, vol. 27, no. 11, pp. 15318–15326, 2019.

[17] H. Zhang, Y. Wang, L. Wang, Y. Liu, H. Chen, and Z. Wu, "Process control monitor (PCM) for simultaneous determination of the piezoelectric coefficients d_{31} and d_{33} of AlN and AlScN thin films," *Micromachines*, vol. 13, no. 4, p. 581, Apr. 2022.

[18] Y. Liu, L. Wang, Y. Su, Y. Zhang, Y. Wang, and Z. Wu, "AlScN piezoelectric MEMS mirrors with large field of view for LiDAR application," *Micromachines*, vol. 13, no. 9, p. 1550, Sep. 2022.

[19] P. Instrumente. (Apr. 17, 2022). *Why Fast Steering Mirrors are Used in Laser Communication/Free Space Optical Communication*. [Online]. Available: https://www.pi-china.cn/zh_cn/knowledge-center/blog/fast-steering-mirrors-for-deep-space/

[20] P. Instrumente. (Apr. 18, 2022). *Piezo Flexure Tilting Mirrors*. [Online]. Available: https://www.pi-china.cn/zh_cn/products/nanopositioning-piezo-flexure-stages/piezo-flexure-tilting-mirrors/

[21] K. L. Turner, S. A. Miller, P. G. Hartwell, N. C. MacDonald, S. H. Strogatz, and S. G. Adams, "Five parametric resonances in a microelectromechanical system," *Nature*, vol. 396, no. 6707, pp. 149–152, Nov. 1998.

[22] C. Pollock, M. Imboden, A. Stange, J. Javor, K. Mahapatra, L. Chiles, and D. J. Bishop, "Engineered PWM drives for achieving rapid step and settle times for MEMS actuation," *J. Microelectromech. Syst.*, vol. 27, no. 3, pp. 513–520, Jun. 2018.

[23] M. Imboden, J. Chang, C. Pollock, E. Lowell, M. Akbulut, J. Morrison, T. Stark, T. G. Bifano, and D. J. Bishop, "High-speed control of electromechanical transduction: Advanced drive techniques for optimized step-and-settle response of MEMS micromirrors," *IEEE Control Syst. Mag.*, vol. 36, no. 5, pp. 48–76, Oct. 2016.

[24] F. Ishola and M. Cho, "Experimental study on photodiode array sensor aided MEMS fine steering mirror control for laser communication platforms," *IEEE Access*, vol. 9, pp. 100197–100207, 2021.

[25] Hamamatsu Photonics. (Aug. 9, 2023). *MEMS Mirrors/Technical Information*. [Online]. Available: https://www.hamamatsu.com.cn/content/dam/hamamatsu-photonics/sites/documents/99_SALES_LIBRARY/ssd/mems_mirror_koth9003e.pdf

WANG YANG received the B.E. degree in physics from Zhejiang University (ZJU), Hangzhou, China, in 2004, the M.S. degree majoring in nuclear technology and application from the Shanghai Institute of Applied Physics, CAS, Shanghai, China, in 2007, and the Ph.D. degree majoring in microelectronics and solid-state electronics from the Shanghai Institute of Technical Physics, CAS, in 2016. He was a Research Associate and an Associate Professor with the IR Sensor Module Division, Shanghai Institute of Technical Physics, from 2007 to 2019. Currently, he is an Associate Professor with the Shanghai Institute of Microsystem and Information Technology (SIMIT), CAS. His research interests include IR sensors, optical MEMS, optical scanning systems, and MEMS LiDAR.

ZHANG YONGGUI received the M.S. degree in measurement and control technology and instrumentation from the North University of China, and the Ph.D. degree from the School of Instrumentation and Optoelectronic Engineering, Beihang University, China, in 2022. Currently, he is a Postdoctoral Researcher with the Shanghai Institute of Microsystem and Information Technology, CAS. His research interests include MOEMS systems and advanced optical sensors.

LIU YICHEN received the B.E. degree in micro electromechanical (MEMS) systems from Northwestern Polytechnical University (NWPU), Xi'an, China, in 2017, and the M.Sc. degree majoring in microsystem from the Karlsruhe Institute of Technology (KIT), Karlsruhe, Germany, in 2020. Currently, she is a Research Assistant with the Shanghai Institute of Microsystem and Information Technology (SIMIT), CAS. Her research interests include optical MEMS devices, X-ray filter, and MEMS process development.

YU ZIHAO received the B.E. degree in automation from the University of Science and Technology of China (USTC), Hefei, China. He is currently pursuing the M.S. degree with the Shanghai Institute of Microsystem and Information Technology (SIMIT), CAS, University of Chinese Academy of Sciences (UCAS). His research interests include micro-electromechanical (MEMS) systems and control algorithms for MEMS devices.

WANG LIHAO received the B.E. degree in electronic packaging technology from Xidian University (XDU), Xi'an, China, in 2015, and the Ph.D. degree majoring in microelectronics and solid-state electronics from the Institute of Semiconductor, CAS, Beijing, China. Currently, he is a Postdoctoral Researcher with the Shanghai Institute of Microsystem and Information Technology, CAS. His research interests include optical MEMS, MEMS resonator, electronic circuits, and systems.

WU ZHENYU received the B.S. degree in physics from Shandong University (SDU), Jinan, China, in 2004, and the M.Sc. and Ph.D. degrees from Ulm University, Ulm, Germany, in 2006 and 2011, respectively. He was a Research and Development Engineer and the Project Manager of MEMS technology with the Automotive Electronics Division, Robert Bosch GmbH, Reutlingen, Germany, from 2011 to 2018. He joined the Shanghai Institute of Microsystem and Information Technology (SIMIT), Chinese Academy of Sciences (CAS), in 2018, as a Professor, where he is currently the Director of the Laboratory of Transducer Technology. He is also a Chief Engineer with the Shanghai Industrial μTechnology Research Institute (SITRI) and a joint Professor with Shanghai University. He has published more than 20 papers and 15 international patents and has coauthored four books. His research interests include advanced micro/nano fabrication technology, optical MEMS microsystems, and new sensors based on quantum effects.

● ● ●